Ordered Materials

Deutsche Ausgabe: DOI: 10.1002/ange.201600675
Internationale Ausgabe: DOI: 10.1002/anie.201600675

A Single-Crystalline Mesoporous Quartz Superlattice

*Takamichi Matsuno[+], Yoshiyuki Kuroda[+], Masaki Kitahara, Atsushi Shimojima, Hiroaki Wada, and Kazuyuki Kuroda**

Abstract: *There has been significant interest in the crystallization of nanostructured silica into α-quartz because of its physicochemical properties. We demonstrate a single-crystalline mesoporous quartz superlattice, a silica polymorph with unprecedentedly ordered hierarchical structures on both the several tens of nanometers scale and the atomic one. The mesoporous quartz superlattice consists of periodically arranged α-quartz nanospheres whose crystalline axes are mostly oriented in an assembly. The superlattice is prepared by thermal crystallization of amorphous silica nanospheres constituting a colloidal crystal. We found that the deposition of a strong flux of Li^+ only on the surface of silica nanospheres is effective for crystallization.*

Facing a severe resource problem of rare metals, the use of materials consisting of abundant elements is demanded in many countries; therefore, silica has attracted much attention because it consists of the first and second abundant elements in the earth's crust.[1] The nanostructural control of silica is useful for various applications, such as catalyst supports,[2] separation media,[3] and photonic crystals.[4] However, the methods for nanostructural control are mostly applicable for amorphous silica.[5] Its crystallization with the retention of the nanostructure is quite difficult. Further functionalization of nanostructured silica giving chemical stability[1] and hardness[6] are expected, if the frameworks are crystallized into nanostructurally controlled α-quartz. Optical[7] and piezoelectric[8] properties are also expected for such single-crystalline α-quartz frameworks.

Amorphous silica crystallizes through melting at very high temperature, or by hydrothermal treatment at 200–400 °C under high pressure (10–30 MPa).[9,10] The original nanostructure and morphology of amorphous silica collapse under such harsh conditions. Because the crystallization temperature is reduced under high pressure, crystallization of mesoporous amorphous silica into mesoporous coesite, stishovite, or quartz at relatively low temperature (300–750 °C) and extremely high pressure (2–12 GPa) has been reported, reinforcing the nanostructures of silica by the formation of amorphous carbon (mesophase pitch) in the mesopores.[11] However, the special apparatus for very high pressure significantly limits the size of materials. In addition, the stability of nanostructured silica under extreme conditions is highly dependent on its nanostructure.[12] Therefore, new methods under simpler and milder conditions are demanded to produce bulk materials.

Flux growth is useful for the preparation of high-quality crystals under ordinary pressure,[13] and it is useful to form bulk crystals and expected to be applicable for various transition-metal oxides. Recently, Sanchez and co-workers have reported pioneering work on the fabrication of nanostructured α-quartz (i.e., porous thin films[14] and periodic arrays of submicrometer-sized hollow shells[15]) by using Sr^{2+} or Ba^{2+} as a flux without reinforcing carbon. Amorphous silica was crystallized into α-quartz, retaining its nanostructure. The crystalline domains were orientated in thin films because of the epitaxial growth,[14] whereas polycrystalline materials were prepared in bulk materials.[15] We hypothesized that the formation of polycrystals is due to the use of a relatively weak flux (Sr^{2+} or Ba^{2+}). It was mentioned in the literature[15] that a strong flux of Li^+ caused total loss of the nanostructure. Therefore, our idea is the use of both an Li^+ flux and a carbon framework for the reinforcement of the nanostructures to produce single-crystalline mesoporous quartz superlattices, using conventional apparatus (Scheme 1 a).

In the reports by Sanchez and co-workers,[14,15] they formed mesopores in the starting amorphous silica. A flux (Sr^{2+} or Ba^{2+}) was embedded in the mesopores, which is effective for close contact of amorphous silica with the fluxes. However, such a method is only applicable for relatively large materials (e.g., silica nanospheres more than 100 nm in size). For example, the smallest particle size of monodispersed silica nanospheres constituting a colloidal crystal is about 12 nm, although that of monodispersed mesoporous silica nanospheres is around 73 nm by our optimized method.[16] Therefore, we propose the following method for nanoconfinement of a Li^+ flux between amorphous silica and a reinforcing carbon framework: $LiNO_3$ was introduced in the interstices of the colloidal crystal. Furfuryl alcohol was subsequently introduced and converted into amorphous carbon. $LiNO_3$-saturated furfuryl alcohol is quite useful to retain the Li^+ flux on the surface of silica nanospheres for effective contact of the Li^+ flux with the amorphous silica nanospheres (Scheme 1 b). If non-saturated furfuryl alcohol is used, all the Li^+

[*] T. Matsuno,[+] M. Kitahara, Prof. Dr. A. Shimojima, Prof. Dr. H. Wada, Prof. Dr. K. Kuroda
Department of Applied Chemistry
Faculty of Science and Engineering, Waseda University
Ohkubo 3-4-1, Shinjuku-ku, Tokyo, 169-8555 (Japan)
E-mail: kuroda@waseda.jp
Homepage: http://www.waseda.jp/sem-kuroda_lab/index-en.html
Dr. Y. Kuroda[+]
Waseda Institute for Advanced Study, Waseda University
Nishiwaseda 1-6-1, Shinjuku-ku, Tokyo, 169-8050 (Japan)
Prof. Dr. K. Kuroda
Kagami Memorial Research Institute for Materials Science and Technology, Waseda University
Nishiwaseda 2-8-26, Shinjuku-ku, Tokyo, 169-0051 (Japan)
[+] These authors contributed equally to this work.

Supporting information for this article can be found under: http://dx.doi.org/10.1002/anie.201600675.

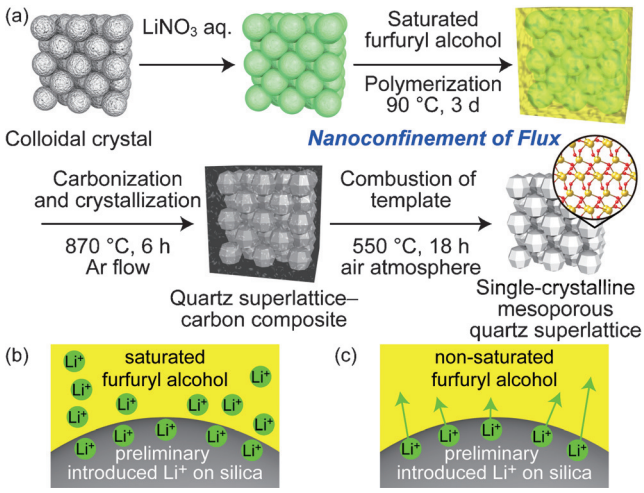

Scheme 1. a) Preparation of a single-crystalline mesoporous quartz superlattice by crystallization of amorphous silica, which constitutes a colloidal crystal, by using a Li^+ flux and a reinforcing carbon framework. b),c) Behaviors of the Li^+ in: b) $LiNO_3$-saturated and c) non-saturated furfuryl alcohol.

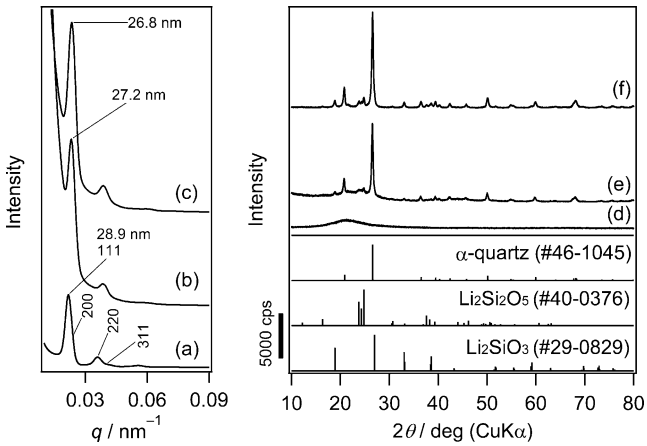

Figure 1. a)–c) SAXS profiles and d)–f) wide-angle XRD patterns of: a),d) the colloidal crystal, b),e) the quartz superlattice-carbon composite, and c),f) the single-crystalline mesoporous quartz superlattice. Bottom: Simulated patters of possible components and their JCPDS card numbers.

flux is dissolved by it and thus trapped inside the carbon framework (Scheme 1 c).

A colloidal crystal consisting of monodispersed silica nanospheres, which was used as a precursor of the single-crystalline mesoporous quartz superlattice, was prepared according to our method.[17] Uniform spherical particles were observed by transmission electron microscopy (TEM; Figure S1(a) in the Supporting Information). Their average size was 32 nm estimated by small-angle X-ray scattering (SAXS) measurements (Figure S2). The standard deviation was 2.3 nm, showing their quite narrow size distribution. After evaporation of the dispersion of silica nanospheres, a colloidal crystal was obtained. The silica nanospheres were arranged in the face-centered cubic (fcc) lattice, confirmed by SAXS (Figure 1 a) and TEM (Figure S1 b–d). The N_2 adsorption–desorption isotherm of the colloidal crystal was type IV (Figure S3 a), showing the presence of interstitial mesopores. The Brunauer–Emmett–Teller (BET) surface area was 120 $m^2 g^{-1}$ and the Barrett–Joyner–Halenda (BJH) pore size was about 10 nm (Figure S3 b). The theoretical surface area of the silica nanospheres is 85 $m^2 g^{-1}$, using 2.2 $g cm^{-3}$ for the density of amorphous silica. The larger surface area than the theoretical value is probably due to surface roughness and/or the relatively low density of the silica nanospheres.

We then sequentially introduced $LiNO_3$ and $LiNO_3$-saturated furfuryl alcohol in the colloidal crystal, followed by heat treatment (see the Experimental Section for detail). Furfuryl alcohol was polymerized and carbonized together with the crystallization of silica nanospheres by heat treatment, and a quartz superlattice-carbon composite was obtained. The wide-angle XRD patterns of the colloidal crystal and the composite show successful crystallization of silica nanospheres (Figure 1 d,e). The sharp peaks are assigned to α-quartz (JCPDS card No. 46-1045). Very small peaks arising from lithium silicates, $Li_2Si_2O_5$ (JCPDS card No. 40-0376) and Li_2SiO_3 (JCPDS card No. 29-0829), were also observed, though they should have little influence on the physicochemical properties of the quartz superlattice because they are basically segregated from a single-crystalline domain. The halo peak of amorphous silica disappeared, and the weak halo at 20–30° is due to amorphous carbon (Figure S4 a,b).

The SAXS profile of the composite indicated diffraction peaks similar to those of the colloidal crystal (Figure 1 b), showing the retention of the regular arrangement of silica nanospheres. The peaks were shifted to higher angle, which indicates shrinkage of the fcc structure by 5.9 % upon heat treatment. The SEM images show that the regular arrangement of the silica nanospheres was retained after the crystallization (Figure S5 a,b). The void space among silica nanospheres was filled with amorphous carbon, which was supported by the observation of a hollow carbon structure like that of an inverse opal[18] on the fractured surfaces (Figure S5 c). The N_2 adsorption–desorption isotherm of the composite showed the absence of the interstitial mesopores between the silica nanospheres (Figure S6).

The reinforcing carbon framework was readily removed by the calcination at 550 °C under air atmosphere. The wide-angle XRD pattern of the single-crystalline mesoporous quartz superlattice shows disappearance of the halo due to amorphous carbon (Figure 1 f, see also Figure S4 c). The peaks arising from α-quartz and lithium silicates were unchanged. The ^{29}Si MAS NMR spectrum of the mesoporous quartz superlattice indicates signals which can be deconvoluted into seven components (Figure S7 a and Table S1). The components at $\delta = -107$ ppm, -92 ppm, and -74 ppm are assignable to α-quartz,[19] $Li_2Si_2O_5$,[20] and Li_2SiO_3,[20] respectively. At least 55 % of the Si atoms formed α-quartz, whereas 17 % of them are included in lithium silicates. Relatively broad components were found at $\delta = -110$ ppm, -100 ppm, and -94 ppm. They may be due to defects in the α-quartz (e.g., surface silanol sites and the neighboring Si atoms). Although such broad signals might be assigned to the original amorphous silica, their half widths (122–170 Hz) are much

narrower than those of the original amorphous silica (ca. 400 Hz, see Figure S7b). The signal at $\delta = -114$ ppm is possibly assignable to minor crystalline silica which did not appear in the XRD patterns.

Intense diffractions arising from the periodic arrangement of silica nanospheres were observed in the SAXS profile (Figure 1c). The shrinkage of the fcc structure was 7.3% from that of the original colloidal crystal. Such sharp and intense peaks for periodic structures have not been observed for other nanostructured α-quartz materials,[11c,14,15] which supports that the present method is effective at retaining the nanostructural order. The periodic arrangement was clearly confirmed by SEM (Figure 2a). The TEM images and the corresponding fast Fourier transform (FFT) images are shown along the [100], [110], and [111] zone axes of the fcc structure (Figure 2b–d). The periodic nanostructure was well retained even after the use of a strong Li^+ flux. Surprisingly, single-crystalline spots owing to α-quartz were observed in the selected area electron diffraction (SAED) patterns (Figure 2e–g).

Figure 2h is a combined TEM image of a flake of the single-crystalline mesoporous quartz superlattice whose size is about $5 \times 2\ \mu m^2$. The TEM image and the FFT pattern indicate that the view direction of the colloidal crystal is $[110]_{CC}$ (subscript of CC means colloidal crystal) in the left side of the flake (Figure 2h1). The view direction is almost $[110]_{CC}$ axis in the right side of the flake with a slight inclination (Figure 2h2). Thus, the flake is almost a single-crystalline colloidal crystal. In most parts of the flake, the SAED patterns showed single-crystalline spots arising from α-quartz along the $[021]_Q$ direction (subscript of Q means α-quartz) (Figure 2h3–h5, h7–h11. Only a small area showed the spots along $[031]_Q$ axis (Figure 2h6) probably a result of local twist. A mixture of the spots along the $[021]_Q$ axis and those along the $[010]_Q$ axis were observed (Figure 2h7, h8, and h9), suggesting local twists and/or the presence of a fractured domain. Accordingly, the flake is almost single-crystalline on both the several tens of nanometer scale and the atomic scale. Such a flake was reproducibly observed (see another result in Figure S8). To our knowledge this is the first report on the detailed characterization of such a double single-crystallinity of silica. Clear relationships between the crystalline orientations of colloidal crystal and α-quartz were not observed.

The quartz superlattice showed the type IV N_2 adsorption–desorption isotherm for the interstitial mesopores (Figure S9a). The BET surface area was $33\ m^2 g^{-1}$, which is smaller than the theoretical value of $70\ m^2 g^{-1}$, using $2.6\ g cm^{-3}$ for the density of α-quartz. The BJH pore size was about 11 nm (Figure S9b). The decrease in the surface area is probably due to the formation of smooth surfaces (Figure 2a), and increase in the neck widths by fusion of silica nanospheres. The formation of non-porous particles should be negligible, based on the SAXS and SEM results. It is the

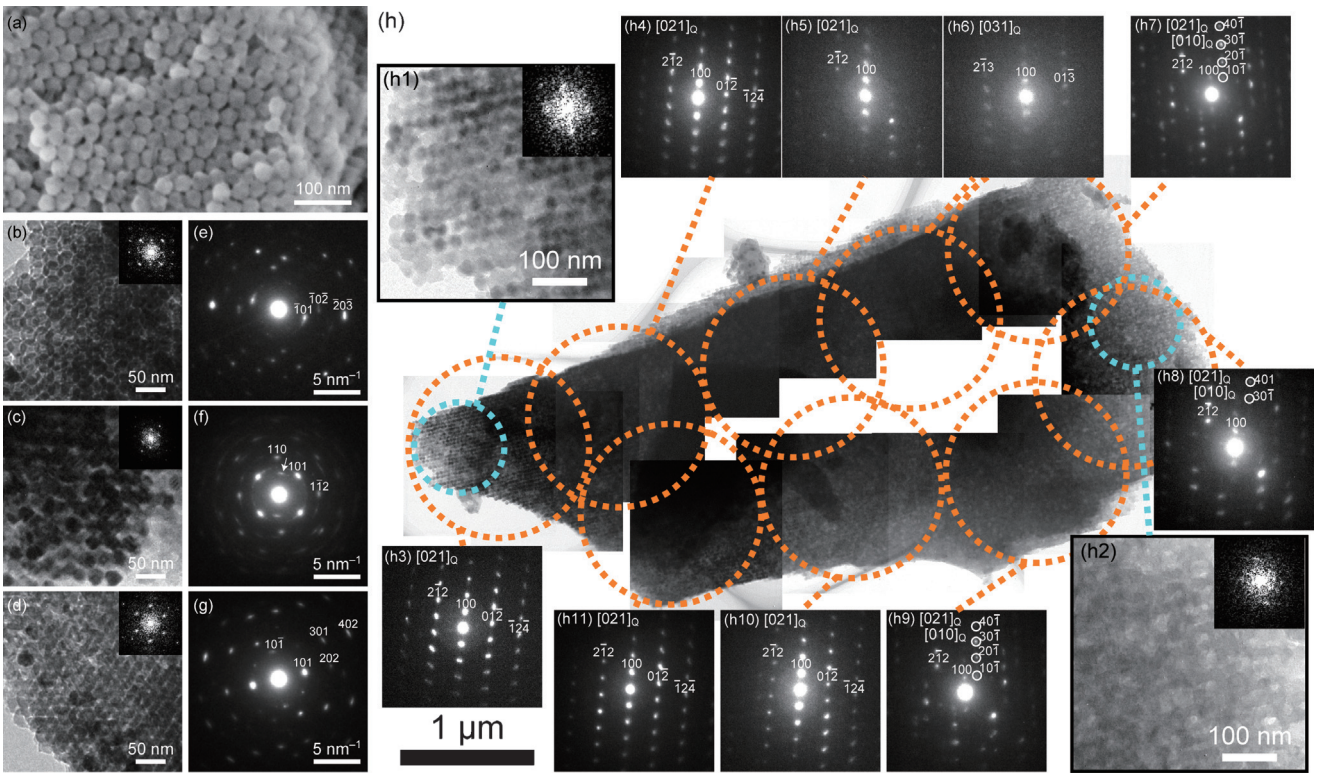

Figure 2. a) SEM image, b)–d) TEM images, and e)–g) the SAED patterns obtained at the same area of the single-crystalline mesoporous quartz superlattice along: b),e) [100], c),f) [110], and d),g) [111] zone axes. The insets in (b)–(d) are the corresponding FFT patterns. The spot due to $Li_2Si_2O_5$ is indicated with an arrow in (f). h) Combined TEM image of the single-crystalline mesoporous quartz superlattice; h1,h2) enlarged images and their corresponding FFT images of a flake from areas in blue circles, and h3–h11) SAED patterns from areas in orange circles. Spots indicated with white circles are due to minor phases.

deviation in the size of the silica nanospheres that is the likely cause of the changes in pore size distributions.

The single crystallinity of the α-quartz structure is explained by efficient melting of silica nanospheres by the strong flux of Li^+. The Si–O bonds in amorphous silica are cleaved into the almost molten state in the nanospace of the carbon framework. Because of the three-dimensional interconnection of the nanospace and the fluidity of molten silica, the silica can crystallize, orienting its axes. The Li^+ flux locating only on the surface of amorphous silica nanospheres is found to be enough for the formation of a single-crystal. Mesoporous non-silica materials with single-crystalline frameworks are also very rare (e.g. gold,[21] TiO_2,[22] and Nb-doped TiO_2[23]). The present method is promising as a general concept for the design of nanostructured materials with single-crystalline frameworks.

The quartz superlattice is expected to be useful as an electrically controllable device, such as photonic crystals[24] and thermal conductors,[25] whose properties are highly dependent on the characteristic length of periodic nanostructures, such as colloidal crystals. The characteristic length is varied by piezoelectric motion arising from the α-quartz framework. It is important to apply the present method for millimeter-sized monolithic colloidal crystals. The piezoelectric motion is also expected to affect guest species incorporated in the interstitial mesopores, which is interesting for novel reactors or quartz oscillators. We applied the method for the crystallization of KIT-6 mesoporous silica, though the periodicity was lost (Figure S10 and the discussion). The thinness and/or low density of the framework of mesoporous silica is probably the reason for the nanostructural collapse. Therefore, the applicability of the method for monoliths, and the effects of thickness and density of frameworks on the crystallization behavior will be studied in the future.

In conclusion, a novel single-crystalline mesoporous quartz superlattice is fabricated by conventional thermal crystallization of amorphous silica nanospheres, constituting a colloidal crystal, by using Li^+ as a strong flux. The nanostructure was successfully retained because of the reinforcement with amorphous carbon. The mesoporous quartz superlattice has single-crystalline periodicity both on the several tens of nanometer scale and the atomic scale with interstitial mesopores. The synthetic method is in principle applicable for various nanostructured amorphous silica. Integration of properties, arising from both length scales, of the newly developed single-crystalline quartz superlattice will be interesting in various fields. We believe the discovery will open a new door for the chemistry and physics of silica.

Experimental Section

Materials: Tris(hydroxymethyl)aminomethane (THAM) and tetraethoxysilane (TEOS) were purchased from Wako Pure Chem. Ind., Ltd. and used without further purification for the synthesis of silica nanoparticles. Lithium nitrate (Wako), furfuryl alcohol (Aldrich), and oxalic acid (Wako) were also used as received. The silica nanospheres and the colloidal crystal were prepared according to our literature.[17]

Crystallization of colloidal crystals: An aqueous solution (0.4 mL) of 0.5 M lithium nitrate was infiltrated into the colloidal crystal (0.3 g). The sample was dried in a desiccator at room temperature for 1 day, then transferred into a Schlenk flask, and vacuum dried at 120 °C for 3 h. After the sample was cooled to room temperature, an excess (1.0 mL) of a furfuryl alcohol solution, saturated with $LiNO_3$ (a large excess of $LiNO_3$ (ca. 0.1 g) was mixed with furfuryl alcohol, followed by the filtration to remove undissolved material) and oxalic acid (0.01 g), was added. $LiNO_3$ was used as a flux and the oxalic acid was used as an acid catalyst for the polymerization of furfuryl alcohol. The Schlenk flask containing the reaction mixture was evacuated for 15 min to maximize the infiltration of the solution. Because the amount of the added solution is very much larger than the volume of interstitial pores, the appearance of the samples shows that the colloidal crystals are almost suspended/dispersed in excess furfuryl alcohol solution. Then, the wet sample was transferred to an alumina boat and the furfuryl alcohol was polymerized at 90 °C for 3 days.[26] The polymer within the composite was carbonized in a tubular furnace under an Ar flow at 870 °C for 6 h. The both heating and cooling rates were 1.7 °C min^{-1}. This procedure is very critical for carbonization of the polymer and the subsequent crystallization of the colloidal crystals. The obtained black sample consisted of crystallized silica nanospheres and a carbon framework. The composite was calcined under air atmosphere at 550 °C for 18 h to remove the carbon framework and form a mesoporous quartz superlattice.

Characterization: TEM images were obtained with a JEOL JEM-2010 microscope at an accelerating voltage of 200 kV. The samples were dispersed in ethanol and dried on a carbon-coated Cu grid. SEM images were also obtained with a Hitachi S-5500 microscope at an accelerating voltage of 3.0 kV. The same samples for the TEM observations were used. SAXS profiles were measured with a Rigaku Nanoviewer system at 40 kV and 30 mA (CuKα radiation), on the camera length 1300 mm with the transmission beam system. Aqueous dispersions were packed in a capillary 1.0 mm in diameter. Powdery samples were mounted on a sample holder with a hole 2 mm in diameter. The particle size was calculated by fitting the SAXS patterns by the Nano-Solver software (Rigaku). Powder XRD patterns were recorded on a Rigaku Ultima III diffractometer at 40 kV and 40 mA (CuKα radiation). N_2 adsorption-desorption isotherms were obtained by a Quantachrome Autosorb-1 instrument at −196 °C. Samples were preheated at 120 °C for 3 h under vacuum. ^{29}Si MAS NMR spectra were recorded on a JEOL JNM-ECX-400 spectrometer at a resonance frequency of 78.65 MHz with a recycle delay of 1000 s by using a 6 mm zirconia rotor and spinning at 5 kHz.

Acknowledgements

We are grateful to Messrs. Minekazu Fuziwara, Toshimichi Shibue, Shinpei Enomoto, Shintaro Hara, Takuya Matsumoto, and Eisuke Yamamoto (Waseda University) for their experimental help and discussion. This work was supported in part by Grants-in-Aid for Scientific Research (No. 26248060 and No. 26810118) and Mizuho Foundation for the Promotion of Science. M.K. thanks for Japan Chemical Industry Association for a fellowship (Human Resources Fostering Program in Chemistry).

Keywords: colloidal crystals · mesoporous silica · single crystals · superlattices · α-quartz

How to cite: *Angew. Chem. Int. Ed.* **2016**, *55*, 6008–6012
Angew. Chem. **2016**, *128*, 6112–6116

[1] R. K. Iler, *The Chemistry of Silica*, Wiley, New York, **1979**.
[2] A. Corma, *Chem. Rev.* **1997**, *97*, 2373.
[3] K. Nakanishi, N. Tanaka, *Acc. Chem. Res.* **2007**, *40*, 863.

[4] D. J. Norris, E. G. Arlinghaus, L. Meng, R. Heiny, L. E. Scriven, *Adv. Mater.* **2004**, *16*, 1393.
[5] Y. Wan, D. Zhao, *Chem. Rev.* **2007**, *107*, 2821.
[6] D. L. Whitney, M. Broz, R. F. Cook, *Am. Mineral.* **2007**, *92*, 281.
[7] a) P. Shumyatsky, R. R. Alfano, *J. Biomed. Opt.* **2011**, *16*, 033001; b) D. Doling, *J. Phys. Chem. Solids* **1979**, *40*, 121; c) Y.-N. Xu, W. Y. Ching, *Phys. Rev. B* **1991**, *44*, 11048.
[8] a) R. K. Cook, P. G. Weissler, *Phys. Rev.* **1950**, *80*, 712; b) C. K. O'Sullivan, G. G. Guilbault, *Biosens. Bioelectron.* **1999**, *14*, 663.
[9] J. F. Bertone, J. Cizeron, R. K. Wahi, J. K. Bosworth, V. L. Colvin, *Nano Lett.* **2003**, *3*, 655.
[10] a) M. Hosaka, *J. Cryst. Growth* **1991**, *112*, 291; b) E. N. Korytkova, L. F. Chepik, T. S. Mashchenko, I. A. Drozdova, V. V. Gusarov, *Inorg. Mater.* **2002**, *38*, 293.
[11] a) P. Mohanty, Y. Fei, K. Landskron, *J. Am. Chem. Soc.* **2009**, *131*, 9638; b) P. Mohanty, V. Ortalan, N. D. Browning, I. Arslan, Y. Fei, K. Landskron, *Angew. Chem. Int. Ed.* **2010**, *49*, 4301; *Angew. Chem.* **2010**, *122*, 4397; c) P. Mohanty, B. Kokoszka, C. Liu, M. Weinberger, M. Mandal, V. Stagno, Y. Fei, K. Landskron, *Microporous Mesoporous Mater.* **2012**, *152*, 214; d) V. Stagno, M. Mandal, K. Landskron, Y. Fei, *Phys. Chem. Miner.* **2015**, *42*, 509.
[12] R. A. Mayanovic, H. Yan, A. D. Brandt, Z. Wang, M. Mandal, K. Landskron, W. A. Bassett, *Microporous Mesoporous Mater.* **2014**, *195*, 161.
[13] P. Armand, A. Lignie, M. Beaurain, P. Papet, *Crystals* **2014**, *4*, 168.
[14] A. Carretero-Genevrier, M. Gich, L. Picas, J. Gàzquez, G. L. Drisko, C. Boissière, D. Grosso, J. Rodriguez-Carvajal, C. Sanchez, *Science* **2013**, *340*, 827.
[15] G. L. Drisko, A. Carretero-Genevrier, A. Perrot, M. Gich, J. Gàzquez, J. Rodriguez-Carvajal, L. Favre, D. Grosso, C. Boissière, C. Sanchez, *Chem. Commun.* **2015**, *51*, 4164.
[16] E. Yamamoto, M. Kitahara, T. Tsumura, K. Kuroda, *Chem. Mater.* **2014**, *26*, 2927.
[17] K.-M. Choi, K. Kuroda, *Chem. Commun.* **2011**, *47*, 10933.
[18] A. A. Zakhidov, R. H. Baughman, Z. Iqbal, C. Cui, I. Khayrullin, S. O. Dantas, J. Marti, V. G. Ralchenko, *Science* **1998**, *282*, 897.
[19] G. Kowalczyk, J. E. Roberts, *Anal. Chim. Acta* **1994**, *286*, 25.
[20] C. Bischoff, H. Eckert, E. Apel, V. M. Rheinberger, W. Höland, *Phys. Chem. Chem. Phys.* **2011**, *13*, 4540.
[21] a) Y. Kuroda, K. Kuroda, *Angew. Chem. Int. Ed.* **2010**, *49*, 6993; *Angew. Chem.* **2010**, *122*, 7147; b) Y. Kuroda, Y. Sakamoto, K. Kuroda, *J. Am. Chem. Soc.* **2012**, *134*, 8684.
[22] E. J. W. Crossland, N. Noel, V. Sivaram, T. Leijtens, J. A. Alexander-Webber, H. J. Snaith, *Nature* **2013**, *495*, 215.
[23] M. Kitahara, Y. Shimasaki, T. Matsuno, Y. Kuroda, A. Shimojima, H. Wada, K. Kuroda, *Chem. Eur. J.* **2015**, *21*, 13073.
[24] F. Marlow, Muldarisnur, P. Sharifi, R. Brinkmann, C. Mendive, *Angew. Chem. Int. Ed.* **2009**, *48*, 6212; *Angew. Chem.* **2009**, *121*, 6328.
[25] J.-K. Yu, S. Mitrovic, D. Tham, J. Varghese, J. R. Heath, *Nat. Nanotechnol.* **2010**, *5*, 718.
[26] T. Yokoi, Y. Sakamoto, O. Terasaki, Y. Kubota, T. Okubo, T. Tatsumi, *J. Am. Chem. Soc.* **2006**, *128*, 13664.

Received: January 21, 2016
Published online: April 6, 2016

